Sensors and Actuators A 186 (2012) 48–53

Contents lists available at SciVerse ScienceDirect

Sensors and Actuators A: Physical

journal homepage: www.elsevier.com/locate/sna

Optimization of a micro Coriolis mass flow sensor using Lorentz force actuation

J. Groenesteijn[a,*], T.S.J. Lammerink[a], R.J. Wiegerink[a], J. Haneveld[b], J.C. Lötters[a,c]

[a] MESA+ Institute for Nanotechnology, University of Twente, Enschede, The Netherlands
[b] Micronit Microfluidics BV, Enschede, The Netherlands
[c] Bronkhorst High-Tech BV, Ruurlo, The Netherlands

ARTICLE INFO

Article history:
Available online 21 January 2012

Keywords:
Micro Coriolis mass flow sensor
Lorentz force actuation
Optimization
Finite Element Analysis

ABSTRACT

In this paper we present Finite Element models to optimize the Lorentz force actuation of a micro Coriolis mass flow sensor. These models specify six different configurations for the permanent magnets used to create the magnetic field for the actuation. The models are used to compare the various configurations in terms of the strength of the Lorentz force used for actuating the vibrational modes, and in terms of the sensitivity to misalignment of the magnetic field of the magnets. The simulations show that the Lorentz force actuation can be increased significantly by improving the placement of the magnets and that the actuation is insensitive to misalignment of the tube in relation to the magnetic field. By applying the models to a fabricated sensor, the magnetic field outside the sensor area has been reduced by 6 orders of magnitude. Due to the smaller size of the new permanent magnets, the footprint of the chip, including actuation, has been reduced by a factor 3. The models of two magnet configurations without misalignment have been validated with measurements.

1. Introduction

We previously presented a micro Coriolis mass flow sensor capable of measuring a flow range of 10 mg/h up to more than 1000 mg/h [1,2]. The sensor uses a vibrating tube to measure the mass flow. This vibration is actuated by the Lorentz force caused by an electrical current through a metal track on top of the tube, which is placed in a magnetic field caused by permanent magnets.

The sensor presented in this paper showed significant improvements compared to earlier work on micro Coriolis mass flow sensors [3,4] in terms of range and accuracy. However, key drawbacks of the design were the large package needed because of the large permanent magnets (12 mm long, 5 mm diameter) and the large magnetic field outside the sensor caused by these magnets. These drawbacks are highly undesirable in the delicate systems the sensor is intended for. Therefore, we investigated the Lorentz actuation in terms of the type of magnets that were used, the placement of the magnets and the influence of misalignment of the magnetic field. Fig. 1 shows a photo of the previously presented sensor with large permanent magnets (Fig. 1a) and the improved design with small (1 mm^3) permanent magnets mounted directly on the chip (Fig. 1b).

2. Theory

2.1. Coriolis mass flow sensing

A Coriolis mass flow sensor uses a vibrating tube to measure the mass flow through the tube. A fluid that flows through the tube results in a small Coriolis force, which can be detected. Fig. 2 shows a schematic drawing of a Coriolis flow sensor based on a rectangular tube shape. The tube is actuated in a torsional mode (also known as twist mode), indicated by angular velocity ω_{am}, by Lorentz force. The mass flow Φ_m through the tube results in a Coriolis force F_C on the tube segment with length L_x along the x-axis. The Coriolis force is calculated using Eq. (1).

$$\vec{F}_C = -2 \cdot L_x \cdot (\vec{\omega}_{am} \times \vec{\Phi}_m) \quad (1)$$

The Coriolis force induces an out-of-plane mode (known as the swing mode) with amplitude proportional to the mass flow. Comb-fingers attached to the tube and to the (static) bulk of the chip form a capacitance that is dependent on the location of the tube relative to the bulk. These comb structures are located on both sides of the rotational axis. For a purely twisting motion, this will result in two periodically changing capacitances that change in anti-phase. A swinging motion will then induce a phase-shift between the two signals, that is proportional to the relative amplitude of the swinging motion. A detailed discussion of the capacitive read-out is presented in [2].

* Corresponding author at: University of Twente, P.O. Box 217, 7500AE Enschede, The Netherlands. Tel.: +31 53 489 4373.
E-mail address: j.groenesteijn@ewi.utwente.nl (J. Groenesteijn).

0924-4247/$ – see front matter © 2012 Elsevier B.V. All rights reserved.
doi:10.1016/j.sna.2012.01.010

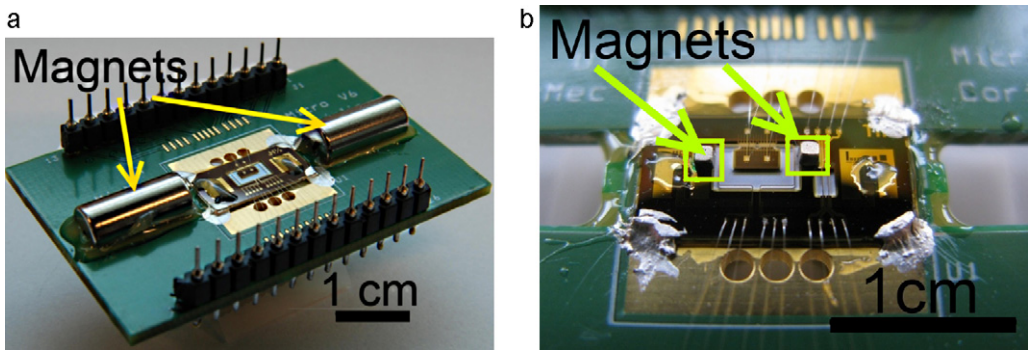

Fig. 1. Photographs of: (a) the previously presented micro Coriolis mass flow sensor with large magnets and (b) the micro Coriolis mass flow sensor with miniature magnets.

2.2. Lorentz actuation

The tube is actuated using Lorentz force actuation. Due to the magnetic field $\vec{B}$, an alternating current $\vec{i}_a$ through a metal track on top of the tube will cause twisting motion around ω_{am}. Ideally, the magnetic field is homogenous over the whole tube area and along the x-axis as shown in Fig. 2. In that case, there will only a Lorentz force on the two tube segments of length L_y along the y-axis and the strength can be calculated using Eq. (2).

$$\vec{F}_L = L_y \cdot (\vec{i}_a \times \vec{B}) \quad (2)$$

The simulations described in Section 3 will analyse the non-ideal case in which the magnetic field is not homogenous.

2.3. Fabrication

The micro Coriolis mass flow sensor consists of a silicon nitride micro channel that is freely suspended over an etched cavity in the silicon substrate. Fig. 3 shows the outline of the fabrication process used to make the sensor. A more detailed description can be found in [5].

Starting with a highly doped ⟨1 0 0⟩ p++ wafer, a 500 nm thick, low-stress LPCVD silicon-rich silicon nitride (Si_xN_y) layer is deposited. Then the fluid inlet/outlet holes are etched from the backside of the wafer using deep reactive ion etching (DRIE). The Si_xN_y layer at the top side is used as etch stop (Fig. 3a). Next, a 1 μm thick TEOS (tetraethyl orthosilicate) oxide layer is deposited and removed from the front side of the wafer. Then a 50 nm layer of chromium is sputtered on the front side of the substrate. This chromium layer is patterned using a mask containing arrays of 5 μm × 2 μm holes, spaced 3 μm apart. This pattern forms the centreline of the final channel. The pattern is then transferred into the nitride layer by reactive ion etching and subsequently the channels are etched in the silicon using isotropic plasma etching (Fig. 3b). The TEOS layer and chromium mask are then removed and another Si_xN_y layer is grown with a thickness of 1.8 μm to form the channel walls and seals the etch holes in the first nitride layer (Fig. 3c). A 10 nm layer of chromium and 200 nm layer of gold are sputtered (chromium serving as the adhesion layer for gold) and patterned to create the metal electrodes for actuation and readout (Fig. 3d). Next, the release windows are opened by reactive ion etching of the Si_xN_y layer (Fig. 3e) and the structure is released by isotropic etching of silicon (Fig. 3f). Fig. 4 shows a SEM photo of a fabricated Coriolis mass flow sensor.

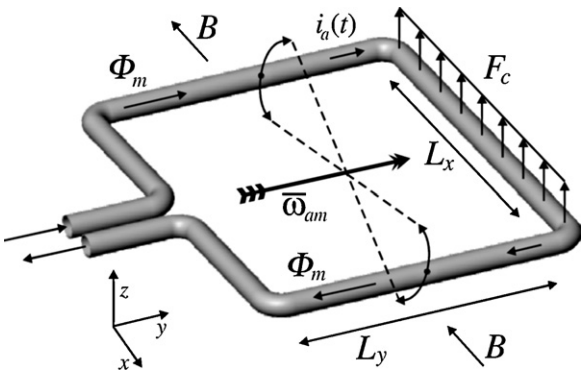

Fig. 2. Schematic view of a micro Coriolis mass flow sensor showing the relevant parameters.

3. Modelling and simulations

3.1. Models

To optimize the Lorentz actuation, Finite Element models were made of several different configurations of both large and miniature magnets to investigate the different influences on the Lorentz force actuation. The six different configurations are shown in Fig. 5. The first configuration has the large permanent magnets of the previously presented sensor. The second configuration with two small magnets has been constructed and measured to compare with the model. A short description of each configuration is given in Table 1. Except for the first configuration, all configurations are based on the use of cube magnets with sides of 1 mm. Further improvements to the magnetic field might be achieved by adding a yoke of high permeability material. However this option has not yet been investigated due to the complexity of implementing such configurations.

From these models, a measure can be found for the actuation of the twist and swing modes. The best configuration will have a high component for the twist mode while it actuates the swing mode as little as possible to minimize crosstalk to the Coriolis sensing. Since the Coriolis force will be 90° out of phase with the Lorentz force, the swing mode that is actuated by Lorentz force can be compensated for in the read-out electronics of the sensor. In practise the actuated swing motion cannot be fully compensated, resulting in a zero-flow offset. The exact influence of this has not yet been investigated. The current analysis focusses mainly on the actuation of the twist

Table 1
Description of the various magnet configurations used in the models, as shown in Fig. 5.

#	Description
1	Two large magnets next to the chip as previously used in the sensor
2	Two miniature magnets on the chip; one on each side of the tube
3	Four miniature magnets on the chip; two on each side of the tube
4	Three miniature magnets on the chip inside the tube area
5	Configuration 3 and configuration 4 combined
6	11 miniature magnets aligned both around and inside the tube area

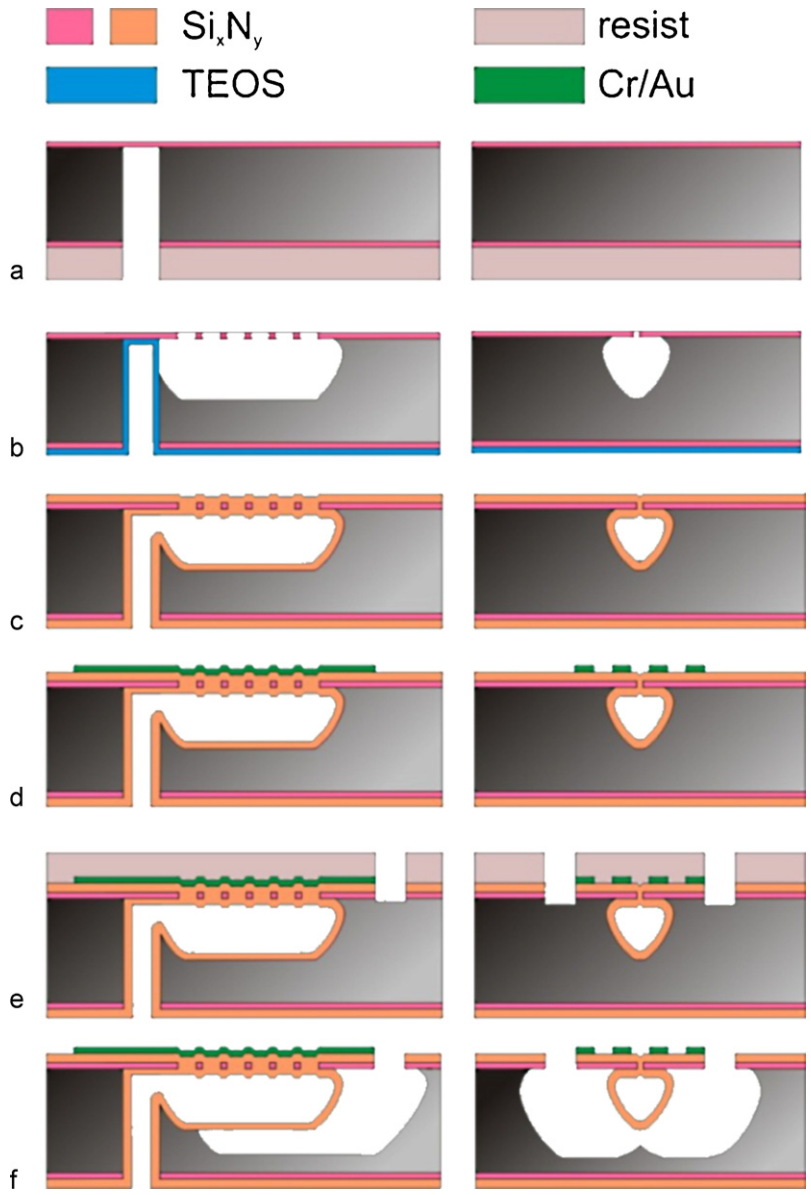

Fig. 3. Schematic view of the fabrication steps. Left: through-wafer cross-section along the length of the tube. Right: through-wafer cross-section of the tube.

mode with a side note that the twist actuation should be as large as possible compared to the actuated swing mode. Section 3.3 shows the simulated effects of misalignments of the magnetic field on the resulting Lorentz force actuation.

The actuation of both vibrational modes will result from a torque around a rotational axis. Fig. 6a and b illustrates this for the twist and swing mode respectively.

The Lorentz force on each part of the tube has to be multiplied by the distance r to the rotational axis to calculate the torque. Since the actuation current in Eq. (2) will always follow the tube, a measure for the strength of the Lorentz actuation can be found by multiplying the component of the magnetic field perpendicular to the tube by the distance to the rotational axis and integrating that over the length of the tube. The resulting torque T for each mode can be calculated using Eq. (3), where r is the distance to the relevant rotational axis an B_p is the component of the magnetic field perpendicular to the tube.

$$T = \int_{\text{Tube}} (r \cdot B_p \cdot |\vec{i}_a|) dx \tag{3}$$

To make the analysis of the different configurations independent of the actuation current, $\vec{i}_a$ is set to unity to remove it from the equation. What is left is a measure for the strength of actuation for the twist and swing modes which can be used to compare the different models.

The residual magnetism $\vec{B}_r$ of the magnets in the models was set according to the specifications of the supplier [6].

3.2. Simulation results

Fig. 7a and b shows the simulated magnetic field strength along the length of the tube multiplied by the distance to the rotational axis for the six different configurations for the twist and swing modes respectively. The horizontal axis is the distance along the tube from the point where it is connected to the bulk of the chip. The values on the x-axis correspond to the values shown in Fig. 6.

These graphs show significant differences for the six different configurations. They also show that, when integrated over the length of the tube, the torque on both sides of the rotational axis for the twist mode will add up, while these torques will partly cancel

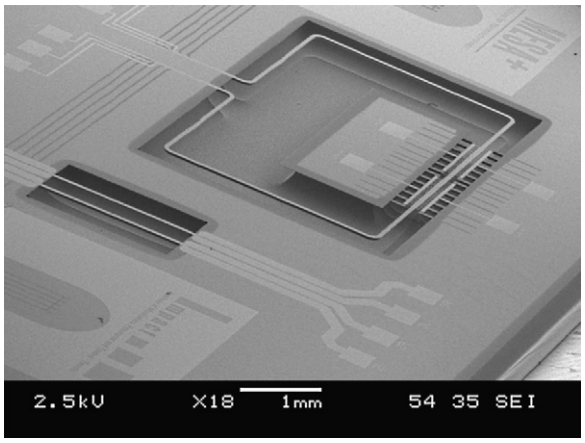

Fig. 4. SEM photo of the micro Coriolis mass flow sensor next to a thermal flow sensor made in the same fabrication process.

each other for the swing mode. A notable difference between the different configurations is that the configurations without a magnet inside the area of the tube create a torque on the long side of the tube with opposite sign to that on the short side on the tube. This means that the Lorentz force on the long and short sides of the tube counteract each other for configurations 1, 2 and 3. Table 2 shows the simulation results when the localized torque is integrated over the length of the tube. To compare the various configurations, the torque for both the twist and the swing actuation is normalized to that of configuration 1. The right column in the table shows the ratio between the twist and swing actuation. The results show that the twist actuation can be increased by a factor of 1.39 using only three miniature magnets. Adding more magnets at the optimum location further increases the twist actuation while the actuation of the swing mode is further reduced. However, the current fabricated chips do not offer sufficient space for magnets inside the tube area. Future designs will allow magnets to be placed inside the tube area.

Table 2
Comparison of the simulation results for the six different magnet configurations.

#	Twist actuation, normalized to configuration 1	Swing actuation, normalized to configuration 1	Ratio between twist and swing actuation
1	1	1	437
2	0.52	0.35	650
3	0.98	1.21	353
4	1.39	−0.89	−685
5	2.37	0.74	1405
6	2.66	0.24	4829

3.3. Misalignment

The simulations results reported in the previous section are made using the ideal situation when all the magnets are aligned symmetrically. However, in reality there is a chance that the magnetic field due to the magnets is not perfectly symmetrical. Possible causes for this include misalignment of the magnets or the magnetization of the magnets, inaccuracies in the fabrication process or an external field that influences the local field of the permanent magnets.

Additional simulations have been done to find the sensitivity to misalignment for each configuration. The misalignments were modelled as a rotation of the tube in relation to the magnets ($\varphi = 0$–5° in steps of 1°) and a displacement in the x- and y-directions ($\Delta x/\Delta y = 0$–0.3 mm in steps of 0.1 mm). The various

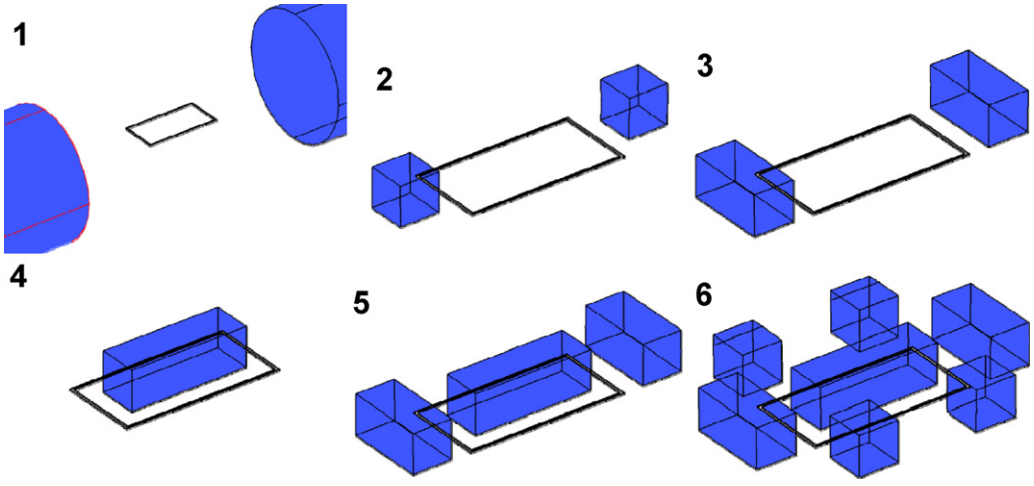

Fig. 5. Schematic view of the six different magnet configurations used in the simulations.

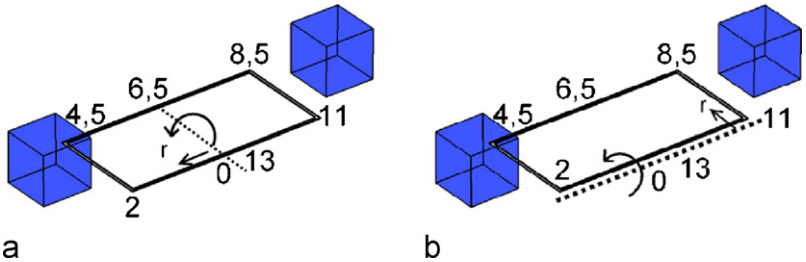

Fig. 6. Schematic view of configuration 2 showing the arm of the rotation axis of the twist (left) and swing (right) modes. The numbers along the tube represent the distances from the starting point in mm.

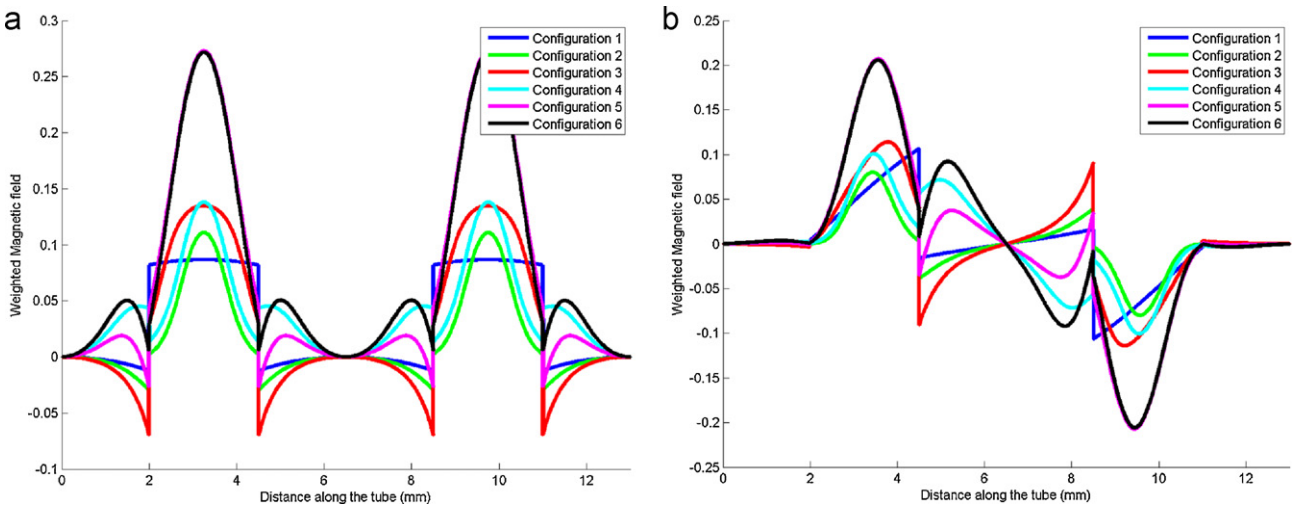

Fig. 7. Simulation results of localized torque for: (a) the twist mode and (b) the swing mode. These values integrated over the complete length of the tube give the torque T as calculated in (3).

Table 3
Simulation results of misalignment in the six different configurations.

#	Normalized twist actuation without misalignment	Relative change in twist actuation with misalignment		
		$\varphi = 5^\circ$	$\Delta x = 0.3$ mm	$\Delta y = 0.3$ mm
1	1	+0.4%	−0.6%	+0.3%
2	0.52	−0.1%	−6.7%	+2.5%
3	0.98	+0.4%	−7.1%	+2.8%
4	1.39	+0.1%@ $\varphi = 3^\circ$	−2.1%	−1.8%
5	2.37	+0.3%	−4.1%	+0.1%
6	2.66	0.04%	−3.2%	−0.8%

types of misalignment are shown in Fig. 8 in a schematic view of configuration 2. Table 3 shows the simulation results compared to the simulations in Section 3.2. The normalized twist actuation without misalignment is shown in the second column. The simulations showed that the effect on the twist actuation increased with increasing misalignment, except for the rotation of configuration 4. The three columns on the right show the relative change of twist actuation found during the simulation of maximum misalignment, compared to the case without misalignment. The table shows that a misalignment does not have a large influence on the strength of the actuation. Except for a displacement in the x-direction, in most cases the actuation of the twist mode increases slightly. During a displacement in the x-direction, the actuation decreases up to 7.1%.

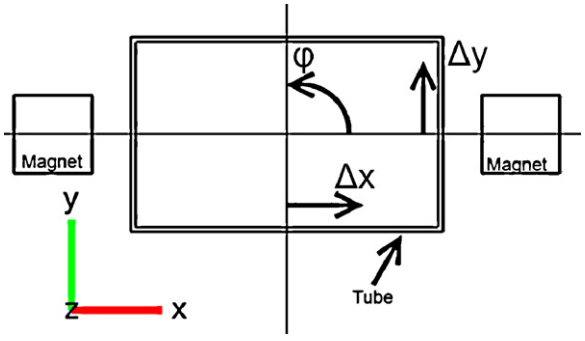

Fig. 8. Schematic view of the three different misalignments that are simulated: rotation (φ) and displacement in x- and y-directions (Δx and Δy respectively).

4. Measurements and discussion

To verify the model, measurements were carried out using sensors fitted with magnets, as in configurations 1 and 2. Two methods were used to compare the magnetic fields. First, using a LakeShore 455 DSP Gauss meter, the magnetic fields of several of both the large and the miniature magnets were measured. The magnetic field on the chip is caused by two magnets. Therefore, to find the total field at each side of the tube, the field had to be measured at various distances from the magnets and summed. For the large magnets, these distances are 8 mm and 12 mm (8 mm + L_x in Fig. 2). For the miniature magnets, these distances are 1 mm and 5 mm. Due to the spread in the magnets, there is some deviation in the magnetic fields for different magnets. For the large magnets the measured total field is 38.5 ± 2.5 mT and 20.75 ± 2.25 mT for the small magnets. Together, this gives a ratio between the fields of 0.54 ± 0.1. The second method for verifying the model was to compare the amplitude of the vibration while applying an alternating current with the same peak-to-peak amplitude. The amplitude of the vibration is proportional to the Lorentz force, which in turn is proportional to the magnetic field. Using this method, a ratio between the field of the miniature magnets and large magnets was found to be 0.59 ± 0.05. The measured values are in accordance with the factor of 0.52 that was predicted by the models.

The measured magnetic field at the edge of the PCB (Fig. 1a and b) was 400 mT when using the large magnets and more than 6 orders of magnitude smaller when using the small magnets. Even directly outside the sensor chip the magnetic field of the two small magnets was only 1 mT. Mass flow measurements presented in [7], which were made using a sensor fitted with the miniature magnets, were compared to mass flow measurements performed using

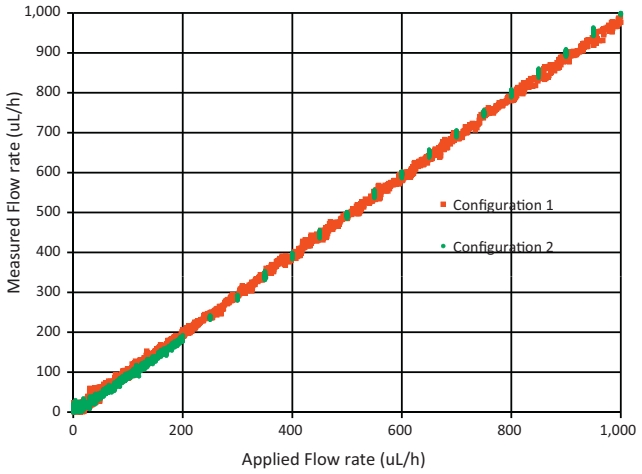

Fig. 9. Mass flow measurements done with micro Coriolis sensors with the magnets configured as in configurations 1 and 2.

a sensor fitted with the large magnets. This comparison shows that the performance of the sensor did not deteriorate due to the smaller magnets. Fig. 9 shows the mass flow measurements done in a range from 10 μl/h up to 1 ml/h. The fluid measured is DI water. The Lorentz actuation current was adjusted in such a way that the amplitude of the twist vibration was equal for both sensors.

5. Conclusion

We investigated the influence of misalignment of six different magnet configurations for Lorentz actuation in order to improve a micro Coriolis mass flow sensor. It has been shown that a significant increase in Lorentz force can be achieved by mounting miniature permanent magnets directly on the chip. At the same time, the magnetic field outside the sensor was reduced by several orders of magnitude.

Misalignment has been modelled by rotating and displacing the tube inside the magnetic fields and the effect on the actuation strength has been investigated. Simulations showed that rotation up to 5° changes the actuation strength by less than 0.5% for all configurations. Displacement of the tube has a larger effect on the actuation but, even in the worst case, still changes the actuation strength by only 7.1%.

Using two miniature magnets (as shown in configuration 2), the magnetic field outside the sensor area is decreased by 6 orders of magnitude compared to the previously presented sensor [1,2,5], while the sensor area required has been reduced by a factor 3. Measurements showed that this had no negative influence on the performance of the sensor.

Acknowledgements

The authors would like to thank the Dutch MicroNed, PIDON-HTF, Kenniswerkers and NanoNextNL Programs for financial support, and the industrial partners for many fruitful discussions. We would also like to thank the reviewers for their valuable comments and recommendations.

References

[1] J. Haneveld, T.S.J. Lammerink, M.A. Dijkstra, H. Droogendijk, M.J. de Boer, R.J. Wiegerink, Highly Sensitive Micro Coriolis Mass Flow Sensor, MEMS, 2008, pp. 920–923.
[2] J. Haneveld, T.S.J. Lammerink, M.J. de Boer, R.J. Wiegerink, Micro Coriolis Mass Flow Sensor with Integrated Capacitive Readout, MEMS, 2009, pp. 463–466.
[3] P. Enoksson, G. Stemme, E. Stemme, A silicon resonant sensor structure for Coriolis mass-flow measurements, J. Microelectromech. Syst. 6 (1997) 119–125.
[4] D. Sparks, R. Smith, J. Cripe, R. Schneider, N. Najafi, A portable MEMS Coriolis mass flow sensor, in: Proc. IEEE. Sensors 2003 Conference, Toronto, Canada, October 22–24, 2003, pp. 90–92.
[5] J. Haneveld, T.S.J. Lammerink, M.J. de Boer, R.G.P. Sanders, A. Mehendale, J.C. Lötters, et al., Modeling, design, fabrication and characterization of a micro Coriolis mass flow sensor, J. Micromech. Microeng. 20 (2010) 125001.
[6] www.supermagnete.de.
[7] T.S.J. Lammerink, J.C. Lötters, R.J. Wiegerink, J. Groenesteijn, J. Haneveld, Single chip flow sensing system with a dynamic flow range of more than 4 decades, Transducers (2011).

Biographies

Jarno Groenesteijn was born in 1985. He received the M.Sc. degree in electrical engineering from the University of Twente, Enschede, The Netherlands, in 2010 on the subject of MEMS-based step-up voltage conversion for comb-drive actuation. Currently he is a Ph.D student at the same university. His work focusses on a micro Coriolis mass flow sensor.

Dr. Ir. Theo S.J. Lammerink received his M.Sc. degree in electrical engineering from the University of Twente, Enschede, The Netherlands, in 1982. From then on he joined the University of Twente as an assistant professor in the field of transducers science. In 1990 he received the Ph.D. degree in electrical engineering at the same university on the subject of 'optical operation of micro-mechanical resonator sensors'. From then on his research focused on micro fluidic systems in general and flow sensors in particular. From 1999 on his interest moved towards conceptual systems analysis and systems modelling. The interest for and research at scientific instrumentation and high level embedded systems has become major part of his activities. Theo Lammerink is author and co-author of about 120 journal and conference papers and several patents.

Dr. Ir. Remco J. Wiegerink received the M.Sc. degree in electrical engineering from the University of Twente, Enschede, The Netherlands, in 1988 on the subject of a fully integrated ultra-low frequency low-pass filter for offset canceling in integrated audio amplifiers. In 1992 he received the Ph.D. degree in electrical engineering at the same university on the subject of MOS translinear circuits. Between 1992 and 1995 he was with the Applied Physics department of the University of Twente, where he was engaged in the design of a superconducting flash analog-to-digital converter with GHz sampling frequency. In 1995 he joined the Transducer Science and Technology (TST) group. Since then his research has focused on mechanical microsensors, electronic interfacing of sensors, and packaging. Highlights include a silicon load cell with distributed capacitive readout, distributed thermal flow sensors using resistor arrays, an RF power sensor based on sensing the electrical force between the signal line, a suspended electrode, flow sensors based on the flow sensing hairs of crickets and a micro Coriolis flow sensor. Remco Wiegerink is (co-) author of two books ("Analysis and Synthesis of MOS Translinear Circuits", and "Mechanical Microsensors"), co-author of several book chapters, and author or co-author of more than 150 journal and conference papers.

Dr. Ir. Jeroen Haneveld was born in Lochem, The Netherlands, in 1977. He received the M.Sc. degree in applied physics in 2001 and the Ph.D. degree in 2006, both from the University of Twente, The Netherlands. His Ph.D. research was aimed at the fabrication and characterization of nanochannels using bond micromachining. After this he spent 4 years as a Post-Doctoral researcher at the Transducers Science and Technology Group (TST) at the University of Twente, designing, fabricating and characterizing a new type of micro Coriolis mass flow sensor. In 2010 he joined Micronit Microfluidics B.V., Enschede, The Netherlands, where he is involved as a R&D project leader in the development of glass- and silicon-based microfluidic systems. Jeroen Haneveld is author or co-author of more than 25 journal and conference papers.

Dr. Ir. Joost C. Lötters received the M.Sc. degree in electrical engineering from the University of Twente, Enschede, The Netherlands, in 1993 on the subject of a buffer amplifier for a piezoelectric impact sensor. In 1997 he received the Ph.D. degree in electrical engineering at the same university on the subject of a highly symmetrical triaxial capacitive accelerometer. In 1997 he joined Bronkhorst High-Tech BV, Ruurlo, The Netherlands. Since then, his research has concentrated on flow measurement and control in the field of thermal and Coriolis flow sensing. In 2010 he joined the Transducer Science and Technology (TST) group as part-time associate professor. Since then his research has focused on microfluidic handling systems. Highlights include a micromachined thermal flow sensor using thermopiles, a micro Coriolis flow sensor and a single chip flow sensing system comprising both a thermal and a Coriolis flow sensor. Joost Lötters is inventor or co-inventor of more than 10 patents and author or co-author of more than 50 journal and conference papers.